The first R_{cr} as a possible measure of the entrainment length in a 2D steady wake

D. Tordella *, S. Scarsoglio

Dipartimento di Ingegneria Aeronautica e Spaziale, Politecnico di Torino, 10129 Torino, Italy

ABSTRACT

At a fixed distance from the body which creates the wake, entrainment is only seen to increase with the Reynolds number (R) up to a distance of almost 20 body scales. This increase levels up to a Reynolds number close to the critical value for the onset of the first instability. The entrainment is observed to be almost extinguished at a distance which is nearly the same for all the steady wakes within the R range here considered, i.e. [20–100], which indicates that supercritical steady wakes have the same entrainment length as the subcritiacal ones. It is observed that this distance is equal to a number of body lengths that is equal to the value of the critical Reynolds number (~ 47), as indicated by a large compilation of experimental results. *A fortiori* of these findings, we propose to interpret the unsteady bifurcation as a process that allows a smooth increase-redistribution of the entrainment along the wake according to the weight of the convection over the diffusion. The entrainment variation along the steady wake has been determined using a matched asymptotic expansion of the Navier–Stokes velocity field [D. Tordella, M. Belan, Phys. Fluids 15 (7) (2003) 1897] built on criteria that include the matching of the transversal velocity produced by the entrainment process.

© 2009 Elsevier B.V. All rights reserved.

1. Introduction

The dynamics of entrainment and mixing is of considerable interest in engineering applications concerning pollutant dispersal or combustion, but it is also of great relevance in geophysical and atmospherical situations. In all these instances, flows tend to be complex. In most cases, entrainment is a time dependent multi-stage process in both the laminar and turbulent regime of motion.

The entrainment of external fluid in a shear flow such as that of a wake or a jet is a convective-diffusive process which is ubiquitous when the Reynolds number is greater than about a decade. It is a key phenomenon associated to the lateral momentum transport in flows which evolve about a main spatial direction. However, quantitative data concerning the spatial evolution of entrainment are not frequent in literature and are difficult to determine experimentally. Quantitative experimental observations are very cumbersome to obtain either in the laboratory or in the numerical simulation context. In some cases, such as, for instance, fluid entrainment by isolated vortex rings, theoretical studies (Maxworthy, 1972 [1]) predate experimental observations (Baird et al., 1977 [2]; Müller and Didden, 1980 [3]; Dabiri and Gharib, 2004 [4]).

It is interesting to note that more attention has been paid to complex unsteady and highly turbulent configurations in literature than to their fundamentally simpler steady counterparts.

In unsteady situations, entrainment is believed to consist of repeated cycles of viscous diffusion and circulatory transport. In turbulent flows, a sequence of processes is observed, where the exterior fluid is first ingested by the highly stretched and twisted interior turbulent motion (large-scale stirring) and is then mixed to the molecular level by the action of the small-scale velocity fluctuations, see for instance the recent experimental works carried out on free jets by Grinstein, 2001 [5] or on a plane turbulent wake by Kopp et al., 2002 [6].

In steady laminar shear flows, stretching dynamics is generally absent (as in 2D flows) or is close to its onset. In this case, entrainment is *determined* by the balance between the longitudinal and lateral nonlinear convective transport and the mainly lateral molecular diffusion.

Air entrainment in free-surface flows is another important instance of the entrainment process. The mechanism is complex and is also significant in nominally steady flows e.g., a waterfall, or a steady jet. In such flows, entrainment is produced through the generation of cavities that can entrap air. The cavities are due to the impingement of the falling jet, which free-surface is usually strongly disturbed, over the liquid surface of the pool. As observed in Ohl et al. 2000 [7], the generation process takes advantage of both the kinetic energy of the jet surface disturbances and of part of the actual energy in the jet.

* Corresponding author.
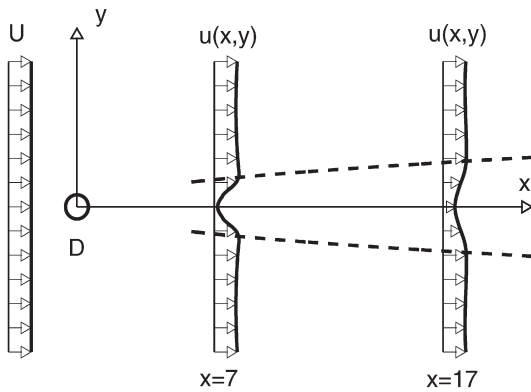*E-mail address:* daniela.tordella@polito.it (D. Tordella).

Fig. 1. Sketch of the physical problem. Longitudinal velocity profiles (solid lines) at $R = 60$ and at stations $x = 7$, $x = 17$.

In this Letter, we consider the steady *two-dimensional* (2D) wake flow past a circular cylinder. We deduce the entrainment as the longitudinal variation of the volume flow defect using a matched Navier–Stokes asymptotic solution determined in terms of inverse powers of the space variables (Belan and Tordella, 2002 [8]; Tordella and Belan, 2003 [9]), see Section 2. This approximated (2D) solution was obtained by recognizing the existence of a longitudinal intermediate region, which introduces the adoption of the thin shear layer hypothesis and supports a differentiation of the behaviour of the intermediate flow with respect to its infinite asymptotics. The streamwise behaviour of the entrainment is presented in Section 3. The concluding remarks are given in Section 4.

2. Analytical approximation of the velocity field, velocity flow rate defect and entrainment

For an incompressible, viscous flow behind a bluff body, the adimensional continuity and Navier–Stokes equations are expressed as

$$u\partial_x u + v\partial_y u + \partial_x p = R^{-1}\nabla^2 u, \tag{1}$$

$$u\partial_x v + v\partial_y v + \partial_y p = R^{-1}\nabla^2 v, \tag{2}$$

$$\partial_x u + \partial_y v = 0 \tag{3}$$

where (x, y) are the adimensional longitudinal and normal coordinates, (u, v) the adimensional components of the velocity field, p the pressure and R the Reynolds number. The physical quantities involved in the adimensionalization are the length D of the body that generates the wake, the density ρ and the velocity U of the free stream, see the flow schematic in Fig. 1. The Reynolds number is defined as $R = \rho U D/\mu$, where μ is the dynamic viscosity of the fluid.

The velocity field for the intermediate region of the 2D steady wake behind a circular cylinder was obtained by matching an inner solution − a Navier–Stokes expansion in negative powers of the inverse of the longitudinal coordinate x

$$f_i = f_{i0}(\eta) + x^{-1/2}f_{i1}(\eta) + x^{-1}f_{i2}(\eta) + \cdots \tag{4}$$

where f is a generic dependent variable and where the quasi-similar transformation $\eta = x^{-1/2}y$ is introduced, and an outer solution, which is a Navier–Stokes asymptotic expansion in powers of the inverse of the distance r from the body

$$f_o = f_{o0}(s) + r^{-1/2}f_{o1}(s) + r^{-1}f_{o2}(s) + \cdots \tag{5}$$

where $r = \sqrt{x^2 + y^2}$ and $s = y/x$.

The wake mass-flow deficit of the inner field was considered by means of an *infield* boundary condition carefully accounting for

it. In fact, this condition is placed at the beginning of the intermediate flow region which inherits the full dynamics properties of near field. To this aim, we took advantage of experimental velocity and pressure profiles, as usually done in many physical contexts and as suggested, in the present context, by Stewartson, 1957 [10]. *Further details about the use of this infield condition are given below.* It should be noted that the matched expansion in ranging from minus infinity to plus infinity in the transversal flow direction and that the concept of wake flow is clearly defined downstream from the intermediate region where the thin layer hypothesis starts to apply. The relevant boundary conditions involve, aside the infield condition, symmetry to the longitudinal coordinate and uniformity at infinity, both laterally and longitudinally. For details on the expansion term determination, the reader can refer to Tordella and Belan, 2003 [9].

The physical quantities involved in the matching criteria are the vorticity, the longitudinal pressure gradients generated by the flow and the transversal velocity produced by the mass entrainment process. The composite expansion is defined as $f_c = f_i + f_o - f_{common}$, where f_{common} is the common part of the inner and outer expansions. In Tordella and Belan, 2003 [9] the explicit inner and outer velocity and pressure expansions can be found up to order four (i.e. $O(x^{-2})$ and $O(r^{-2})$, for the inner and outer wake, respectively), the composite approximation has been shown graphically. In this work, we approximate the wake flow with the composite solution obtained by truncating the inner and outer expansions at the third order term and then by determining their common part by taking the inner limit of the outer approximation. For the reader's convenience, the inner and outer velocity component expansion terms are listed below (see Eqs. (9)–(23)). The common part has not been included because it has an analytical representation which alone would take up a few pages. However, the ©*Mathematica* file that describes its analytical structure and which allows its computation is given in the EPAPS online repository (see Supplementary material). The common expansion was obtained by writing the inner and outer expansions in the primitive independent variables and by taking the inner limit of the outer expansion, that is, by taking the limit for $s \to 0$ and $r \to \infty$. To this end, the Laurent series of the outer expansion about $x \to \infty$ was considered up to the first order. The composite expansion − which is, by construction, a continuous curve, since it is obtained by the *additive composition* of three continuous curves, the sum of the inner and outer expansions minus the part they have in common − is accurate if the common expansion is accurate. This is always obtained if, at each order, the distance $\delta_n = |f_{i,n} - f_{o,n}|$ between the inner and the outer expansions is bounded and is at most of the same order as the range of f_i and f_o. In the present matching, we have verified that in the matching region − that is, in the region where the composite connects the inner and the outer expansions − the distance δ_n is not only bounded, but is small with respect to the ranges of f_i and f_o.

The velocity approximation is shown in Figs. 2 and 3, where the longitudinal and transversal components of the composite solution for the velocity field are plotted for different longitudinal stations and Reynolds numbers.

It should be noted, that in this analytical flow representation, a few key properties of the wake flow have been taken into account. These properties can help an accurate description of the entrainment process to be obtained. These properties are:

(i) The existence of *intermediate asymptotics* for the wake flow, in the general sense as given by Barenblatt and Zeldovich [11]. This is an important point, because the existence of the intermediate region supports the adoption of the thin shear layer hypothesis and relevant near-similar variable transformations for the inner flow, while, at the same time, it also supports a differentiation of
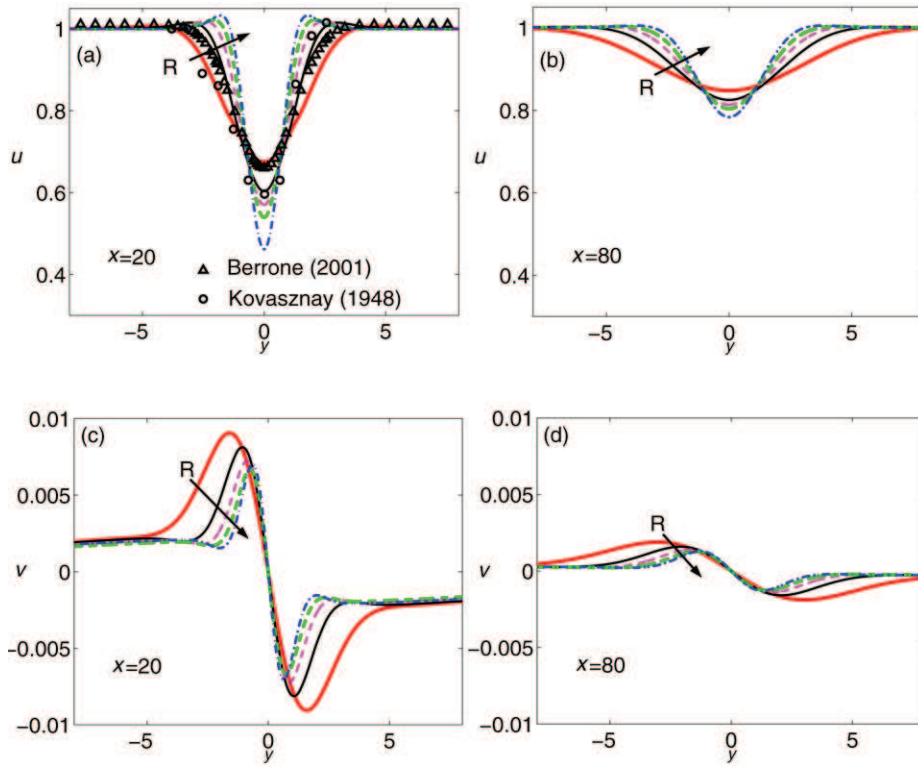
Fig. 2. Velocity profiles at the downstream stations $x = 20$, $x = 80$ and for $R = 20, 40, 60, 80$ and 100. (a), (b) Longitudinal velocity u, $x = 20$ and $x = 80$, (c), (d) transversal velocity v, $x = 20$ and $x = 80$. The comparison with the numerical results by Berrone (2001) (triangles, $R = 34$, $x = 20$) and the laboratory data by Kovasznay (1948) (circles, $R = 34$, $x = 20$) is shown in part (a).
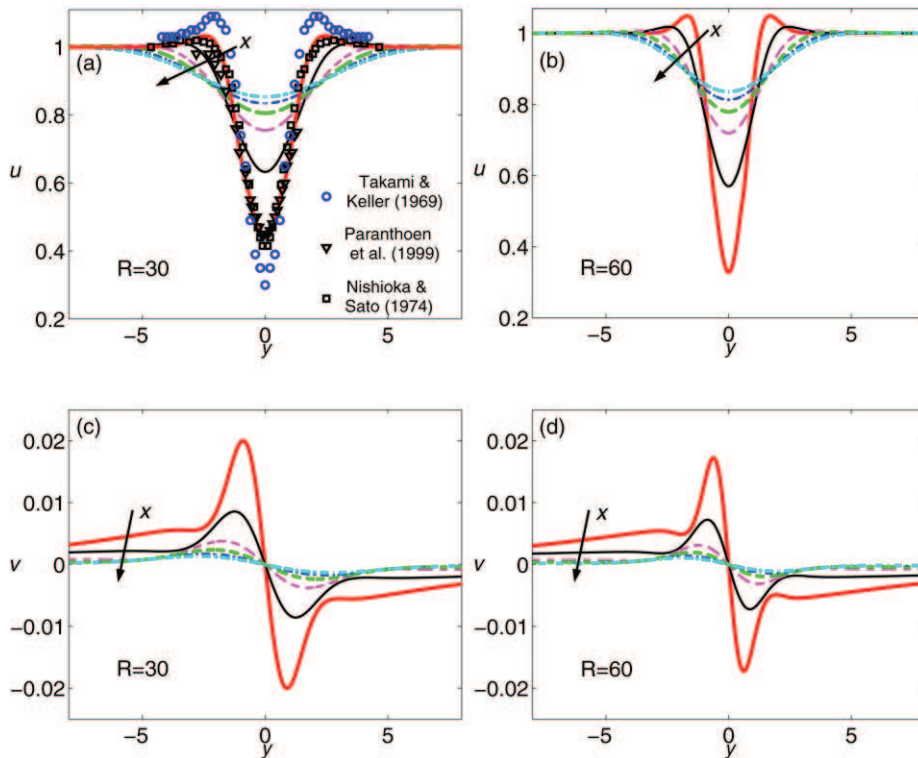
Fig. 3. Velocity profiles for $R = 30, 60$ plotted at stations $x = 10, 20, 40, 60, 80$ and 100. (a), (b) Longitudinal velocity u, $R = 30$ and $R = 60$, (c), (d) transversal velocity v, $R = 30$ and $R = 60$. The comparison with the experimental data by Nishioka and Sato (1974) (squares, $R = 40$, $x = 7$), Paranthoen et al. (1999) (triangles, $R = 34$, $x = 10$) and Takami and Keller (1969) (circles, $R = 40$, $x = 7$) is shown in part (a).

the behavior of the intermediate flow with respect to its infinite asymptotics (Oseen's flow).

(ii) The use of an *in-field* boundary condition which consists of the distribution of the momentum and pressure at a given section along the mainstream of the flow in opposition to the use of integral field quantities. This kind of boundary condition is not new in literature [10], and presents the evident advantage of having a higher degree of field information with respect to the use of integral quantities such as the drag or the lift coefficients (a given integral value can be obtained from many different distributions).

(iii) The acknowledgment of the fact that in free flows, such as low Reynolds numbers − 2D or axis-symmetric − wakes or jets developing in an otherwise homogeneous and infinite expanse of a fluid, the main role in shaping the flow is played by the inner flow. This directly inherits the main portion of the convective and diffusive transport of the vorticity, which is created, at the solid boundaries, by the motion of the fluid relative to the body. For these flows, it is physically opportune to denote the "inner" flow as the straightforward or basic approximation. This means that, up to the first order, the inner solution is independent of the outer solution. According to this, the Navier–Stokes model, coupled with the thin layer hypothesis, very naturally yields the order of the field pressure variations $O(x^{-2})$. Pressure variations were often overestimated at $O(x^{-1})$ [9,12]. This was due to the use, in the inner expansion, of the assumption that the field can accommodate an inner pressure which is independent of the lateral coordinate, which however varies at the leading orders along the x coordinate. However, at intermediate values of y and for fixed x, this assumption is responsible for an anomalous rise in the composite expansion, due to the central plateau that appears in the outer expansion. The outer solution is in fact biased at finite values of x to values greater than 1 and forces the composite expansion to assume inaccurate values − with respect to experimental results − mostly in the region around $y/D \approx 2$ and outwards (at $y/D = 20$ the longitudinal velocity is still appreciably different from U). For details, the reader may refer to Section IV and Fig. 6 in Tordella and Belan, 2003 [9].

(iv) Last, we would like to point out that we have used the Navier–Stokes equations in the whole field, without the addition of any further restrictive axiomatic position, such as the principle of exponential decay. This did not prevent our approximated solution from spontaneously showing the properties of rapid decay and irrotationality at the first and second orders for the inner and the outer flows, respectively. At the higher orders, which mainly influence the intermediate region, the decay becomes a fast algebraic decay.

For an unitary spanwise length, the defect of the volumetric flow rate D is defined as

$$D(x) = \int_{-\infty}^{+\infty} \left(1 - u(x, y)\right) dy \qquad (6)$$

and is approximated through $u_c = u_c(x, y)$, *the composite solution for the velocity field*, as

$$D(x) \approx \int_{-\infty}^{+\infty} \left(1 - u_c(x, y)\right) dy. \qquad (7)$$

Entrainment is the quantity that takes into account the variation of the volumetric flow rate in the streamwise direction, and is defined as

$$E(x) = \left| \frac{dD(x)}{dx} \right|. \qquad (8)$$

The sequence of the first four terms of the inner and outer approximation for the streamwise velocity and the transversal velocity is given in the following.
Zero order, $n = 0$,

$$u_{i0}(x, y) = c_0, \qquad (9)$$

$$v_{i0}(x, y) = 0, \qquad (10)$$

$$u_{o0}(x, y) = k_0, \qquad (11)$$

$$v_{o0}(x, y) = 0 \qquad (12)$$

with $c_0 = 1$, $k_0 = 1$.
First order, $n = 1$

$$u_{i1}(x, y) = -A c_1 e^{-Ry^2/(4x)} x^{-1/2}, \qquad (13)$$

$$v_{i1}(x, y) = 0, \qquad (14)$$

$$u_{o1}(x, y) = 0, \qquad (15)$$

$$v_{o1}(x, y) = 0 \qquad (16)$$

with $c_1 = 1$, while the constant A is related to the drag coefficient ($A = \frac{1}{4}(R/\pi)^{1/2} c_D(R)$).
Second order, $n = 2$

$$u_{i2}(x, y) = -\frac{1}{2} A^2 e^{-Ry^2/(4x)} \left[e^{-Ry^2/(4x)} + \frac{1}{2} \frac{y}{\sqrt{x}} \sqrt{\pi R}\, \text{erf}\left(\frac{1}{2}\sqrt{\frac{R}{x}} y\right) \right] x^{-1}, \qquad (17)$$

$$v_{i2}(x, y) = -\frac{A}{2} \frac{y}{\sqrt{x}} e^{-Ry^2/(4x)} x^{-1}, \qquad (18)$$

$$u_{o2}(x, y) = 0, \qquad (19)$$

$$v_{o2}(x, y) = 0. \qquad (20)$$

Third order, $n = 3$

$$u_{i3}(x, y) = A^3 e^{-Ry^2/(4x)} \left(2 - R\frac{y^2}{x}\right) \left[\frac{1}{2} c_3 - R F_3(x, y)\right] x^{-3/2},$$

$$v_{i3}(x, y) = -\frac{A^2}{2} \left\{ -\frac{1}{2} \frac{y}{\sqrt{x}} e^{-Ry^2/(2x)} - \sqrt{\frac{\pi}{2R}}\, \text{erf}\left(\sqrt{\frac{R}{2x}} y\right) \right.$$
$$\left. + \left(\frac{1}{2}\sqrt{\frac{\pi}{R}} - \frac{\sqrt{\pi R}}{4}\frac{y^2}{x}\right) e^{-Ry^2/(4x)}\, \text{erf}\left(\frac{1}{2}\sqrt{\frac{R}{x}} y\right) \right\} x^{-3/2},$$

$$u_{o3}(x, y) = R\left(\frac{i}{3} k_{31} e^{(3i/2)\arctan(s)} + k_{33}\frac{s_+^{3/2}}{s^{3/2}} + \frac{1}{2} k_{32} s^{-3/2} s_+^{3/2} \right.$$
$$\times \left\{ \frac{\sqrt{(1+is)s}(\frac{3}{4} - \frac{i}{i+s})}{2(i+s)} + \frac{(-1)^{1/4}}{16\sqrt{2}} \right.$$
$$\left.\left. \times \log\left[\frac{(\frac{i-1}{\sqrt{2}} + \sqrt{s})(\frac{i-1}{\sqrt{2}} - (1-i)\sqrt{1+is} + \sqrt{s})}{(\frac{1-i}{\sqrt{2}} + \sqrt{s})(\frac{1-i}{\sqrt{2}} + (1-i)\sqrt{1+is} + \sqrt{s})} \right] \right\} \right),$$

$$v_{o3}(x, y) = R\left(e^{(3i/2)\arctan(s)} \left[k_{31} + k_{32} s^+ \frac{s+i}{3(s-i)^2} \right] \right) \qquad (21)$$

where $c_3 = -2.26605 + 0.15752R - 0.00265R^2 + 0.00001R^3$, F_3 is the third order of the function

$$F_n(x, y) = \frac{1}{\sqrt{x}} \int_0^y \frac{e^{R\zeta^2/(4x)}}{\text{Hr}_{n-1}^2(x, \zeta) G_n(x, \zeta)} d\zeta, \qquad (22)$$

$$G_n(x, y) = A^{-n} \frac{1}{\sqrt{x}} \int_0^y M_n(x, \zeta) \text{Hr}_{n-1}(x, \zeta)\, d\zeta \qquad (23)$$

where $M_n(x, y)$ is the sum of the non-homogeneous terms of the general ordinary differential equation for the inner solution coefficients (ϕ_n), $n \geqslant 1$, obtained from the x component of the Navier–Stokes equation [8,9], and $Hr_{n-1}(x, y) = H_{n-1}(\frac{1}{2}\sqrt{\frac{R}{x}}y)$, where H_n are Hermite polynomials. In the outer terms, the variables $r, s, s^{\pm}$ are defined as $r = \sqrt{x^2 + y^2}$, $s = y/x$, $s^{\pm} = (1+s^2)^{\pm 1/2}$ and the relevant constants are $k_{31} = \pm\frac{1}{2}A^2/2\sqrt{\pi/(2R)}$, $k_{32} = 3ik_{31}$, $k_{33} = 0$.

3. Discussion of the results

Before describing the entrainment features we have observed, let us first discuss the asymptotic behaviour of the inner expansion in the lateral far field, since this aspect is important to determine the entrainment decay. At finite values of x, the inner streamwise velocity decays to zero as a Gaussian law for $n = 1$ and as a power law of exponent -2 for $n = 2$ and of exponent -3 for $n \geqslant 3$. The cross-stream inner velocity goes to zero for $n = 0, 1$ and to a constant value for $n \geqslant 2$. This allows v to vanish as $x^{-3/2}$ for $x \to \infty$. When $x \to \infty$ this approximation coincides with the Gaussian representation given by the Oseen approximation. It can be concluded that, at Reynolds numbers as low as the first critical value and where the non-parallelism of the streamlines is not yet negligible, the division of the field into two basic parts — an inner vortical boundary layer flow and an outer potential flow — is spontaneously shown up to the second order of accuracy ($n = 1$). At higher orders in the expansion, the vorticity is first convected and then diffused in the outer field. This is the dynamical context in which the entrainment process takes place.

In Figs. 2(a) and 3(a), the longitudinal velocity profiles are contrasted with the experimental data available for steady flows, the Direct Numerical Simulations by Berrone, 2001 [13], and Takami and Keller, [14] (see also Figs. 8 and 9 in [16]), and the laboratory data by Paranthoen et al., 1999 [15], Nishioka and Sato, 1974 [16] and Kovasznay, 1948 [17]. The accuracy on the velocity distributions, between the analytical data and the laboratory ones is lower than 5%. This estimate was obtained by contrasting the longitudinal velocity distribution u with the laboratory and numerical distributions, considered as the reference distribution. To this end, we computed the deviation $\Delta_{\text{ref}} = \|u - u_{\text{ref}}\|_{0,x}/\|1 - u_{\text{ref}}\|_{0,x}$. At $R = 34$, a deviation $\simeq 4.5\%$ was obtained for the laboratory results by Kowasznay, where x is the station at 20 diameters from the center of the cylinder, see Fig. 2. As for the data by Berrone, we find a Δ_{ref} of about 1.7%. At $x \sim 10$ we have a comparison with Paranthoen et al., Takami and Keller, and Nishioka and Sato, that yields a deviation Δ_{ref} of about 2.5%, 5% and 1.5%, respectively, see Fig. 3.

The entrainment is closely linked to the lateral and far field asymptotic behaviour. Since a numerical experiment cannot be over an unbounded domain of a flow, this approach is not suitable for the study of the field asymptotic behaviour and, as a consequence, entrainment (however, numerical simulations can yield very accurate representations of the near field, in particular of the standing eddy region). As far as entrainment is concerned, we then contrasted our analytical data with laboratory data. We tried to exploit all the results available in literature, obtaining a comparison with Paranthoen et al., 1999 [15] and Kovasznay, 1948 [17] because these authors present a sequence of velocity profiles (mainly in supercritical flow configurations) that extend into the intermediate wake. The comparison was instead not feasable with the data by Nishioka and Sato, 1974 [16] since they mainly measured the near wake (standing eddy region).

Fig. 4 shows the volumetric flow rate defect $D = D(x; R)$ and the entrainment $E = E(x; R)$ obtained from the composite expansion. It can be observed that the volumetric defect flow rate slowly decreases with the distance from the body (Fig. 4(a)). This decrease is faster at the beginning of the intermediate wake and at the higher Reynolds values. Considering a fixed position x (Fig. 4(c)), the flow defect decreases with the Reynolds number. Fig. 4(a) includes data from the laboratory experiments by Paranthoen et al. (1999, $R = 53.3$) and Kovasznay (1948, $R = 56$), both carried out at a slight supercritical R (unsteady regime). The difference between their results in not small, but it should be recognized that the difficulties in measuring at small values of the Reynolds number are exceptionally high. By considering the arithmetic mean between these two sets of data, an increase of more than 50% with regards to the values of the steady configuration, for $x < 20$, is observed. It is also observed that the numerical simulation by Takami and Keller (1969, $R = 40$) compare very well with the experiment by Paranthoen et al.

Parts (b), (d) of Fig. 4 concern the entrainment, that is, the spatial rate of change of the wake velocity defect. The important points are: – the initial high variation at the beginning of the intermediate part of the wake, which increases with R, – the higher experimental mean value near $x = 10$ (2.45×10^{-2} against 6.5×10^{-3}), – for all the R, the exhaust of the entrainment at a distance of about 50 body lengths, – the collection of experimentally determined values of the critical R number that has a median value of 46.6: a fact that relates the entrainment exhaust length — EEL — to R_{cr} with a simple scaling, such as EEL $\sim R_{\text{cr}}^n$ with $n = 1$. In Fig. 4(d), one can also observe that at a constant distance x from the body, the entrainment stops growing beyond around R_{cr}.

Though the connection between the entrainment length and the instability cannot be direct: – the first can be deduced as an integral property of the steady fully nonlinear version of the motion equations, – the second from the linear theory of stability, which is conceived to highlight the role of the perturbation characteristics and not of the integral properties of the basic flow, these results could be *a fortiori* used to interpret the bifurcation to the unsteady flow condition at R_{cr} as a process that allows the wake to tune the entrainment, and, possibly, to redistribute it on a larger wake portion, according to the actual R value.

It can be noticed that the decay distance is of the same order of magnitude as R_{cr} and this shows that the scaling used in recent stability analyses [18,19] to represent the slow time and space wake evolution — $\tau = \varepsilon t$ and $\xi = \varepsilon x$, where $\varepsilon = \frac{1}{R} \sim \frac{1}{R_{\text{cr}}}$ — is linked to the exhaust of the entrainment process. In fact, one can say that the unit value of the slow time and spatial scales is reached where the entrainment nearly ends.

4. Conclusions

The entrainment is observed to be intense in the intermediate wake downstream from the separation region where the two-symmetric standing eddies are situated. Here, the dependence on the Reynolds number is clear. The entrainment grows six-fold when R is increased from 20 to 100. The subsequent downstream evolution presents a continuous decrement of the entrainment. For all the R here considered, it has been observed that this decrease is almost accomplished at a distance from the body of about 50 diameters, which is a value that is close to the critical value R_{cr} for the onset of the first instability and the subsequent set up of the unsteady regime (the median value in literature being $R_{\text{cr}} = 46.6$). The establishment of the unsteady regime could be interpreted as a way of overcoming the limitation on the entrainment intensity and decay imposed by the steady regime. The observed decay length confirms the validity of the scaling that is often adopted in wake stability studies carried out using the spatial and temporal multitasking approach.
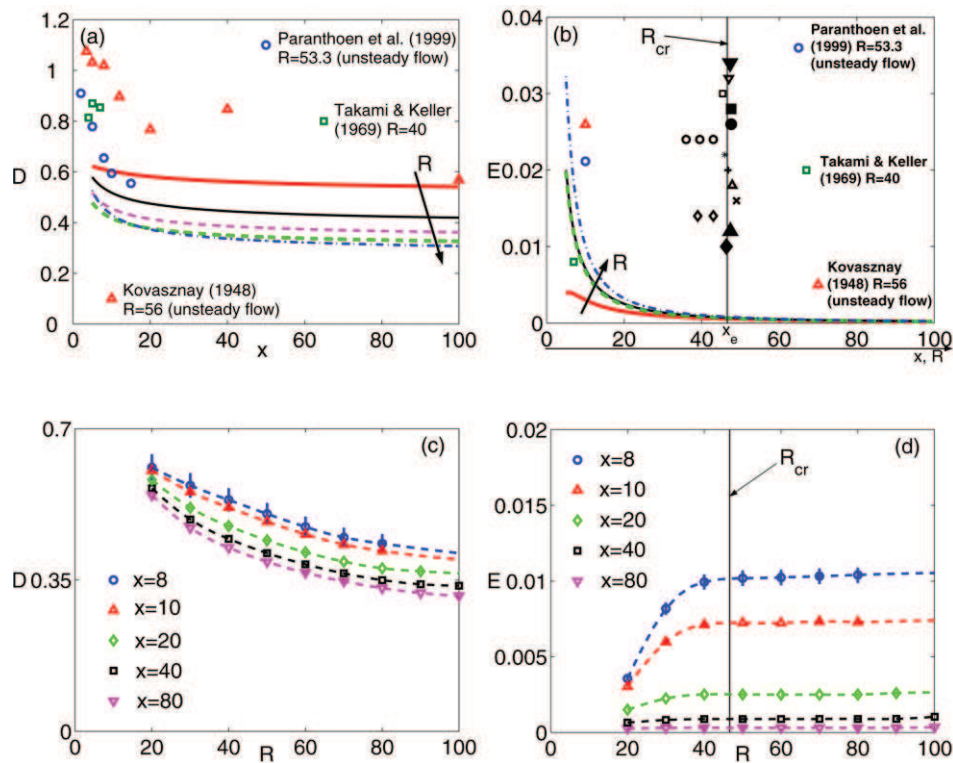
Fig. 4. (a), (b): Downstream distribution of the volumetric flow rate defect D and entrainment E for $R = 20, 40, 60, 80$ and 100. (c), (d): Volumetric flow rate defect D and entrainment E as a function of the R for different stations ($x = 8, 10, 20, 40, 80$). The values of the volumetric flow rate defect D for the oscillating (supercritical) wake, as inferred from experimental data by Kovasznay (1948, $R = 56$), Takami and Keller (1969, $R = 40$) and Paranthoen et al. (1999, $R = 53.3$), are also shown in part (a). The values of the critical Reynolds number obtained from different numerical and experimental results are placed at a distance from the body, x_e, equal to R_{cr}, see part (b). Position x_e is observed to be the wake length where the entrainment is almost extinguished $\forall R \in [20, 100]$, which leads to the hypothesis that the steady wake becomes unstable at a Reynolds number that is equal to the normalized distance where the entrainment almost ends and to the value beyond which the entrainment, at a constant distance from the body, stops growing (see part (d)). The symbols represent data from: Norberg, 1994 [20] (▲), Zebib, 1987 [21] (◇), Pier, [22] 2001, (×), Williamson, [23] 1989 (△), Leweke and Provansal, [24] 1995 (+), Strykowski and Sreenivasan, [25] 1990 (∗), Coutanceau and Bouard, [26] 1977 (○), Elsenlhor and Eckelmann, [27] 1989 (●), Hammache and Gharib, [28] 1989 (■), Jackson, [29] 1987 (□), Ding and Kawahara, [30] 1999 (◆), Morzynski et al., [31] 1999 (▽), Kumar and Mittal, [32] 2006 (▼). The solid line in parts (b) and (d) indicates the median value ($R_{cr} \approx 46.6$) of these data.

Acknowledgements

Supplementary material

Online version of this Letter contains ©*Mathematica* supplemental file: EPAPS-TS-WAKE-ENTRAINMENT.nb.

Please visit DOI: 10.1016/j.physleta.2009.01.063.

References

[1] T. Maxworthy, J. Fluid Mech. 51 (1972) 15.
[2] M.H.I. Baird, T. Wairegi, H.J. Loo, Can. J. Chem. Engrg. 55 (1977) 19.
[3] E.A. Müller, N. Didden, Stroj. Casop. 31 (1980) 363.
[4] J.O. Dabiri, M. Gharib, J. Fluid Mech. 511 (2004) 311.
[5] F.F. Grinstein, J. Fluid Mech. 437 (2001) 69.
[6] G.A. Kopp, F. Giralt, J.F. Keffer, J. Fluid Mech. 469 (2002) 49.
[7] C.D. Ohl, H.N. Oguz, A. Prosperetti, Phys. Fluids 12 (7) (2000) 1710.
[8] M. Belan, D. Tordella, Z. Angew. Math. Mech. 82 (4) (2002) 219.
[9] D. Tordella, M. Belan, Phys. Fluids 15 (7) (2003) 1897.
[10] K. Stewartson, J. Math. Phys. 36 (1957) 173.
[11] G.I. Barenblatt, Y.B. Zel'dovich, Annu. Rev. Fluid Mech. 4 (1972) 285, doi:10.1146/annurev.fl.04.010172.001441.
[12] I. Chang, J. Math. Mech. 10 (1961) 811.
[13] S. Berrone, Comput. Methods Appl. Mech. Engrg. 190 (34) (2001) 4435.
[14] H. Takami, H.B. Keller, Phys. Fluid Suppl. II 12 (1969) 51.
[15] P. Paranthoen, L.W.B. Browne, S. Le Masson, F. Dumouchel, J.C. Lecordier, Eur. J. Mech. B/Fluids 18 (1999) 659.
[16] M. Nishioka, H. Sato, J. Fluid Mech. 65 (1) (1974) 97.
[17] L.S.G. Kovásznay, Proc. R. Soc. London Sect. A 198 (1948) 174.
[18] D. Tordella, S. Scarsoglio, M. Belan, Phys. Fluids 18 (5) (2006).
[19] M. Belan, D. Tordella, J. Fluid Mech. 552 (2006) 127.
[20] C. Norberg, J. Fluid Mech. 258 (1994) 287.
[21] A. Zebib, J. Eng. Math. 21 (1987) 155.
[22] B. Pier, J. Fluid Mech. 458 (2002) 407.
[23] C.H.K. Williamson, J. Fluid Mech. 206 (1989) 579.
[24] T. Leweke, M. Provansal, J. Fluid Mech. 288 (1995) 265.
[25] P.J. Strykowski, K.R. Sreenivasan, J. Fluid Mech. 218 (1990) 71.
[26] M. Coutanceau, R. Bouard, J. Fluid Mech. 79 (1977) 231.
[27] H. Eisenlhor, H. Eckelmann, Phys. Fluids A-Fluid Dyn. 1 (1989) 189.
[28] M. Hammache, M. Gharib, Phys. Fluids A-Fluid Dyn. 1 (1989) 1611.
[29] C.P. Jackson, J. Fluid Mech. 182 (1987) 23.
[30] Y. Ding, M. Kawahara, Int. J. Numer. Methods Fluids 31 (1999) 451.
[31] M. Morzynski, K. Afanasiev, F. Thiele, Comput. Methods Appl. Mech. Engrg. 169 (1999) 161.
[32] B. Kumar, S. Mittal, Comput. Methods Appl. Mech. Engrg. 195 (2006) 6046.